Available online at http://scik.org
Commun. Math. Biol. Neurosci. 2025, 2025:119
https://doi.org/10.28919/cmbn/9452
ISSN: 2052-2541

STOCHASTIC DIFFERENTIAL EQUATIONS FOR SIR MALARIA MODEL

A. OKWOMI SHARON[1,*], SAMUEL CHEGE MAINA[1,2], COLLINS OJWANG' ODHIAMBO[1,3], SAMUEL MWALILI[1]

[1]Strathmore Institute for Mathematical Sciences, Strathmore University, Nairobi, Kenya

[2]Microsoft Research Lab – Africa, Nairobi, Kenya

[3]Department of Paediatrics, College of Medicine,University of Illinois,Peoria, IL, United States

Abstract. This study develops a stochastic extension of the classical SIR malaria model to more realistically capture the dynamics of malaria transmission under environmental uncertainty. By incorporating Brownian motion into the deterministic framework, the model accounts for random fluctuations in transmission and recovery processes affecting both human and mosquito populations. The stochastic differential equations (SDEs) are solved using three numerical methods: Euler–Maruyama, Milstein, and Stochastic Runge–Kutta. Each method is evaluated for accuracy and reliability using error metrics such as Mean Absolute Deviation (MAD), Root Mean Square Error (RMSE), and the Anderson–Darling goodness-of-fit test. The Euler–Maruyama method demonstrates superior performance in approximating human infection and recovery dynamics, while the Milstein method provides a balanced estimate for both human and vector compartments. The study further introduces a novel convergence metric–Okwomi C^*–based on the Geweke diagnostic, enabling robust assessment of convergence in stochastic simulations. Simulation results show that stochastic models capture extinction and variability effects not evident in deterministic models, even when the basic reproduction number exceeds one. Overall, the integration of stochastic processes improves epidemic forecasting and informs more resilient malaria control strategies under uncertainty.

Keywords: Bayesian inference; stochasticity; Wiener process; convergence measure.

2020 AMS Subject Classification: 60H10, 92D30.

*Corresponding author

E-mail address: sharonokwomi@gmail.com

Received June 26, 2025

1. INTRODUCTION

Epidemiology encompasses the systematic investigation of disease distribution patterns and their determinants, with particular emphasis on modelling approaches to evaluate intervention strategies for disease control. Of specific interest are vector-borne diseases such as malaria, which present complex transmission dynamics.

Mathematical modelling serves as a cornerstone in modern epidemiology, providing robust frameworks for quantifying transmission dynamics, recovery rates, mortality, and other epidemiological parameters. The field's mathematical foundations can be traced to Bernoulli's seminal work in 1760 [1], which established the first formal mathematical treatment of epidemic processes. Subsequently, the contributions of Anderson and May [2, 3] have demonstrated the essential role of mathematical models in generating testable hypotheses and informing evidence-based predictions about disease outbreaks. These models have evolved to become instrumental in public health policy formulation and implementation.

The Susceptible-Infected-Recovered (SIR) model, introduced by Kermack and McKendrick in 1927 [4], represents a fundamental framework in infectious disease modelling. This compartmental model is characterized by the following system of differential equations:

$$\begin{cases} \frac{dS}{dt} = \mu N - \beta S(t)I(t) - \mu S(t) \\ \frac{dI}{dt} = \beta S(t)I(t) - (\gamma + \mu)I(t) \\ \frac{dR}{dt} = \gamma I(t) - \mu R(t) \end{cases} \tag{1}$$

where:

(1) $S(t)$, $I(t)$, and $R(t)$ represent Susceptible, Infected, and Recovered populations.

(2) μ denotes natural birth/death rate.

(3) β represents transmission rate.

(4) γ indicates recovery rate.

(5) $N = S(t) + I(t) + R(t)$ is total population.

Although the SIR model provides a powerful deterministic framework for understanding disease dynamics, it assumes perfect predictability given initial conditions. However, real-world epidemiological processes exhibit inherent randomness. Stochastic models incorporate this variability through probabilistic elements, offering a more nuanced representation of disease transmission dynamics.

This paper focuses on developing a stochastic epidemiological model for malaria transmission, employing a single Brownian motion process to capture environmental stochasticity. The research aims to demonstrate the advantages of stochastic modelling approaches in epidemiological contexts, particularly for understanding the complex dynamics of vector-borne diseases.

2. Model Formulation

Epidemiological modelling has traditionally relied on deterministic SIR frameworks [4]. However, real-world disease transmission is inherently stochastic, influenced by environmental fluctuations, demographic variation, and other random factors [5]. This work establishes a general framework for incorporating environmental stochasticity through Brownian motion, providing a more realistic representation of disease dynamics.

Wiener Process. A stochastic process $\{W(t)\}_{t\geq 0}$ is called a Wiener process or a Brownian motion if

(1) $W(0) = 0$.

(2) $\{W(t)\}_{t\geq 0}$ has independent increments, i.e.

$$W_{t_1}, W_{t_2} - W_{t_1}, \ldots, W_{t_k} - W_{t_{k-1}}$$

are independent random variables for all $0 \leq t_1 < t_2 < \cdots < t_k$.

(3) $W(t+s) - W(s) \sim \mathcal{N}(0,t)$ for all $t > 0$.

Here,$\mathcal{N}\left(\mu, \sigma^2\right)$ denotes the normal distribution with mean μ and variance σ^2. Thus, the Wiener process is a Gaussian process. The Wiener process is continuous with mean zero and variance proportional to the elapsed time: $\mathbb{E}(W(t)) = 0$ and $\text{Var}(W(t)) = t$. If $\{X(t)\}_{t\geq 0}$ is a stationary stochastic process, then $\{X(t)\}_{t\geq 0}$ has the same distribution as $\{X(t+h)\}_{t\geq 0}$ for all $h > 0$.

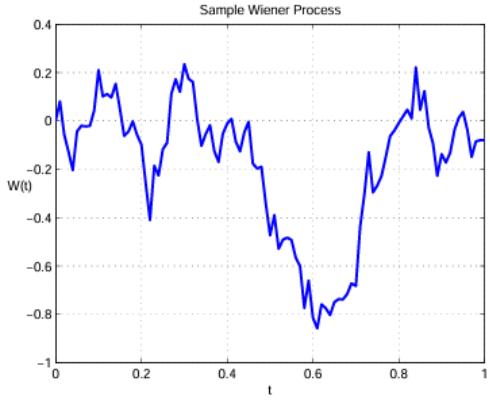

(A) Sample Wiener process with a small number of steps ($n = 100$) to compute at $t \in [0,1]$.

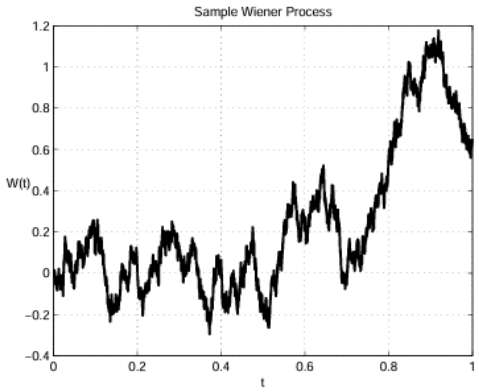

(B) Sample Wiener process with a high number of steps ($n = 10000$) to compute at $t \in [0,1]$.

FIGURE 1. Comparison of Wiener processes with different step sizes.[6]

Figures 1a and 1b, demonstrates the inherent stochastic nature of the Wiener process $W(t)$ which serves as a mathematical framework for incorporating uncertainties into deterministic differential equations. These comparative illustrations show the distinct behavioural characteristics of the Wiener process under varying computational resolutions within the interval $[0,1]$. The numerical analysis suggests that implementing a fine temporal discretization through increased iterations or reduced step size is essential for adequately capturing the system's stochastic fluctuations. Conversely, when employing coarser temporal resolution through reduced iterations or enlarged step size, the process exhibits behaviour that more closely approximates deterministic dynamics, potentially overlooking important stochastic features of the system [6].

SDE in general. In general, assume that the ODE

$$\frac{dx}{dt} = a(x,t)$$

describes a one-dimensional dynamical system. Assume that $a(\cdot)$ fulfils conditions such that a unique solution exists, thus $x(t) = x(t;x_0,t_0)$ is a solution satisfying the initial condition $x(t_0) = x_0$. Given the initial condition, we know how the system behaves at all times t, even if we cannot find a solution analytically. We can always solve it numerically up to any desired precision. In many biological systems this is not realistic, and a more realistic model can be obtained if we allow for some randomness in the description.

A natural extension of a deterministic ODE model is given by an SDE model, where relevant parameters are randomized or modelled as random processes of some suitable form, or simply by adding a noise term to the driving equations of the system. This approach assumes that some degree of noise is present in the dynamics of the process. Here we will use the Wiener process. It leads to a mixed system with both a deterministic and a stochastic part in the following way:

$$dX_t = \mu\left(X_t, t\right) dt + \sigma\left(X_t, t\right) dW_t$$

where $\{X_t = X(t)\}_{t\geq 0}$ is a stochastic process, not a deterministic function. This is indicated by the capital letter. Here $\{W_t = W(t)\}_{t\geq 0}$ is a Wiener process and since it is nowhere differentiable, we need to define what the differential means. It turns out that it is useful to write $dW_t = \xi_t dt$, where $\{\xi_t\}_{t\geq 0}$ is a white noise process, defined as being normally distributed for any fixed t and uncorrelated: $E\left(\xi_t \xi_s\right) = 0$ if $s \neq t$. Strictly speaking, the white noise process $\{\xi_t\}_{t\geq 0}$ does not exist as a conventional function of t, but could be interpreted as the generalized derivative of a Wiener process.

The functions $\mu(\cdot)$ and $\sigma(\cdot)$ can be non-linear, $\mu(\cdot)$ is called the drift coefficient or the deterministic component, and $\sigma(\cdot)$ is called the diffusion coefficient or the stochastic component (system noise), that may depend on the state of the system, X_t. If $\mu(\cdot)$ and $\sigma(\cdot)$ do not depend on t the process is called time-homogeneous. Equation (1.3) should be interpreted in the following way:

$$X_t = X_0 + \int_{t_0}^{t} \mu\left(X_s, s\right) ds + \int_{t_0}^{t} \sigma\left(X_s, s\right) dW_s$$

where X_0 is a random variable independent of the Wiener process.

SDE SIR Model. The traditional deterministic SIR model is given by c.f Eq (1). We introduce environmental stochasticity through Brownian motion:

$$\begin{cases} dS = (\mu N - \beta S(t)I(t) - \mu S(t))dt - \sigma_1 S(t)I(t)d\beta_t \\ dI = (\beta S(t)I(t) - (\gamma+\mu)I(t))dt + \sigma_2 S(t)I(t)d\beta_t \\ dR = (\gamma I(t) - \mu R(t))dt \end{cases} \tag{2}$$

where:

(1) $d\beta_t$ represents the increment of standard Brownian motion.

(2) σ_1, σ_2 denote noise intensities.

(3) The condition $\sigma_1 = \sigma_2$ ensures population conservation.

Theorem 1. *For the stochastic SIR system* [5]*, if* $\sigma_1^2 < 2\beta$*, then:*

(1) Solutions exist and are unique.

(2) Solutions remain non-negative.

(3) $\mathbb{E}[S(t) + I(t) + R(t)] = N$

The stochastic basic reproduction number is defined as:

$$\mathscr{R}_0^S = \mathscr{R}_0 - \frac{\sigma^2}{2\beta^2} \tag{3}$$

where $\mathscr{R}_0 = \frac{\beta N}{\gamma+\mu}$ is the deterministic basic reproduction number.

The incorporation of Brownian motion in SIR models provides several advantages:

(1) Captures environmental fluctuations.

(2) Accounts for parameter uncertainty.

(3) Provides more realistic epidemic predictions.

(4) Enables risk assessment through probability distributions.

SDE Malaria Model.

SIR Malaria Model. This section presents a mathematical formalization of the malaria transmission dynamics. The human population dynamics are modelled using the SIR malaria model framework, accounting for the absence of permanent immunity and the possibility of reinfection. In contrast, the vector population follows a Susceptible-Infected (SI) model, reflecting the biological observation that mosquitoes, due to their relatively brief lifespan, do not recover from parasitic infection.

The model incorporates several key epidemiological characteristics: temporary immunity in recovered human hosts with subsequent return to susceptibility, universal susceptibility of newborns to infection, and disease transmission initiated by the bite of an infectious female Anopheles mosquito. Notably, the parasitic infection remains nonlethal to the vector population and does not impact vector fitness.

This compartmental framework captures the essential biological and epidemiological characteristics of the host-vector system while maintaining mathematical tractability for analysis of disease dynamics and control strategies.

SDE SIR Malaria Model. We extend the classical SIR malaria model by incorporating environmental stochasticity through Brownian motion. The analysis demonstrates that stochastic perturbations significantly affect disease dynamics and extinction probabilities, providing more realistic predictions than deterministic. We consider a compartmental model that divides the human population into three classes: susceptible S_h, infected I_h and recovered R_h, while the mosquito population is divided into susceptible S_m and infected I_m classes. The model incorporates vital dynamics (births and deaths) for both populations. The system of ordinary differential equations describing the dynamics is given by:

$$
\begin{aligned}
\frac{dS_h}{dt} &= -\alpha_h S_h - \beta_h S_h I_m + \pi_h \\
\frac{dI_h}{dt} &= -(\alpha_h + \gamma_h + \rho_h - \delta_h) I_h + \beta_h S_h I_m \\
\frac{dR_h}{dt} &= -\alpha_h R_h + \gamma_h I_h \\
\frac{dS_m}{dt} &= -\alpha_m S_m - \beta_m S_m I_h + \pi_m \\
\frac{dI_m}{dt} &= -\alpha_m I_m + \beta_m S_m I_h
\end{aligned}
\tag{4}
$$

where:

- α_h, α_m represent natural death rates for humans and mosquitoes.
- β_h, β_m are transmission/contact rates.
- γ_h is the human recovery rate.
- ρ_h is the disease-induced death rate.
- δ_h represents infected migration rates for humans.
- π_h, π_m are the birth / recruitment rates of humans and mosquitoes.

The model satisfies the biological constraints $N_h(t) \leq \frac{\pi_h}{\alpha_h}$ and $N_m(t) \leq \frac{\pi_m}{\alpha_m}$ for all $t > 0$, ensuring bounded populations [7].

Stochastic Extension With Environmental Noise. To account for environmental fluctuations that affect disease transmission, we extend the deterministic model by incorporating Brownian motion terms [8]. The resulting system of stochastic differential equations is as follows:

$$
\begin{aligned}
dS_h &= (-\alpha_h S_h - \beta_h S_h I_m + \pi_h)dt - \sigma_1 S_h I_m dW_{1t} \\
dI_h &= [-(\alpha_h + \gamma_h + \rho_h - \delta_h)I_h + \beta_h S_h I_m]dt + \sigma_2 S_h I_m dW_{2t} \\
dR_h &= (-\alpha_h R_h + \gamma_h I_h)dt - \sigma_3 R_h dW_{3t} \\
dS_m &= (-\alpha_m S_m - \beta_m S_m I_h + \pi_m)dt - \sigma_4 S_m I_h dW_{4t} \\
dI_m &= (-\alpha_m I_m + \beta_m S_m I_h)dt + \sigma_5 S_m I_h dW_{5t}
\end{aligned} \tag{5}
$$

where $W_{jt},\ j = 1,2,\cdots,5$ are independent standard Brownian motions, and $\sigma_j,\ j = 1,2,\cdots,5$ represent the intensities of environmental noise in the five (5) SDEs [9].

3. General Form of Cholesky for Correlation Matrix

Let $\mathbf{P} \in \mathbb{R}^{5\times 5}$ be the correlation matrix of the Wiener processes $dW_{1t}, dW_{2t}, dW_{3t}, dW_{4t}, dW_{5t}$, where:

$$P_{ij} = \rho_{ij}, \quad \rho_{ii} = 1$$

We want to construct a lower triangular matrix $\mathbf{L}$ such that

$$\mathbf{P} = \mathbf{L}\mathbf{L}^\top$$

and then use this $\mathbf{L}$ to map independent Brownian motions $d\mathbf{Z}_t$ to correlated ones $d\mathbf{W}_t = \mathbf{L}d\mathbf{Z}_t$.

For $n = 5$, the Cholesky matrix $\mathbf{L}$ is lower triangular:

$$\mathbf{L} = \begin{bmatrix} \ell_{11} & 0 & 0 & 0 & 0 \\ \ell_{21} & \ell_{22} & 0 & 0 & 0 \\ \ell_{31} & \ell_{32} & \ell_{33} & 0 & 0 \\ \ell_{41} & \ell_{42} & \ell_{43} & \ell_{44} & 0 \\ \ell_{51} & \ell_{52} & \ell_{53} & \ell_{54} & \ell_{55} \end{bmatrix}$$

We compute each ℓ_{ij} recursively so that $\mathbf{L}\mathbf{L}^\top = \mathbf{P}$. The pattern follows:

Diagonal terms:

$$\ell_{ii} = \sqrt{1 - \sum_{k=1}^{i-1} \ell_{ik}^2}$$

Off-diagonal terms (for $i > j$):

$$\ell_{ij} = \frac{1}{\ell_{jj}} \left(\rho_{ij} - \sum_{k=1}^{j-1} \ell_{ik} \ell_{jk} \right)$$

We'll fill in symbolic entries for the first few rows, similar to your image.

Let's define:

- $\rho_{12}, \rho_{13}, \rho_{14}, \rho_{15}$
- $\rho_{23}, \rho_{24}, \rho_{25}$
- ρ_{34}, ρ_{35}
- ρ_{45}

and assume symmetry (i.e., $\rho_{ij} = \rho_{ji}$).

Then the Cholesky factor $\mathbf{L}$ becomes:

$$\mathbf{L} = \begin{bmatrix} 1 & 0 & 0 & 0 & 0 \\ \rho_{12} & \sqrt{1-\rho_{12}^2} & 0 & 0 & 0 \\ \rho_{13} & \dfrac{\rho_{23}-\rho_{12}\rho_{13}}{\sqrt{1-\rho_{12}^2}} & \sqrt{1-\rho_{13}^2-\left(\dfrac{\rho_{23}-\rho_{12}\rho_{13}}{\sqrt{1-\rho_{12}^2}}\right)^2} & 0 & 0 \\ \ell_{41} & \ell_{42} & \ell_{43} & \ell_{44} & 0 \\ \ell_{51} & \ell_{52} & \ell_{53} & \ell_{54} & \ell_{55} \end{bmatrix}$$

The stochastic model exhibits fundamentally different behavior from its deterministic counterpart [10]. Even when the deterministic basic reproduction number $R_0 > 1$, the disease can go extinct with positive probability due to random fluctuations. The probability of extinction depends on both the initial conditions and the intensities of the noise [5].

4. METHODS

This section examines the Euler–Maruyama, Milstein, and Runge–Kutta methods for solving stochastic differential equations in the SIR model framework. We compare stochastic and deterministic versions of the SIR model tailored to the Kenyan context. By varying white noise

intensity, we assess how stochasticity influences disease dynamics. We examine both random and deterministic simulations to offer a clearer picture of how randomness affects infectious disease modeling, enhancing our understanding of epidemic behavior under uncertain conditions.

Stochastic Taylor Expansion. The Stochastic Taylor Expansion generalizes the classical Taylor series to SDEs, incorporating terms that capture randomness from Brownian motion. Consider the one-dimensional Itô stochastic differential equation (SDE):

$$X_t = X_{t_0} + \int_{t_0}^{t} a(X_s)\,ds + \int_{t_0}^{t} b(X_s)\,dW_s,$$

where $a(x)$ and $b(x)$ are smooth functions and W_t is a standard Brownian motion.

For a twice continuously differentiable function $f : \mathbb{R} \to \mathbb{R}$, Itô's formula states:

$$f(X_t) = f(X_{t_0}) + \int_{t_0}^{t} \left(a(X_s) f'(X_s) + \frac{1}{2} b^2(X_s) f''(X_s) \right) ds + \int_{t_0}^{t} b(X_s) f'(X_s)\,dW_s.$$

Define the operators:

$$L^0 = a\frac{d}{dx} + \frac{1}{2} b^2 \frac{d^2}{dx^2}, \quad L^1 = b\frac{d}{dx}.$$

Then the equation can be compactly written as

$$f(X_t) = f(X_{t_0}) + \int_{t_0}^{t} L^0 f(X_s)\,ds + \int_{t_0}^{t} L^1 f(X_s)\,dW_s.$$

Applying Itô's formula recursively to $f = a$ and $f = b$ yields:

$$\begin{aligned} X_t = X_{t_0} &+ \int_{t_0}^{t} \left(a(X_{t_0}) + \int_{t_0}^{s} L^0 a(X_z)\,dz + \int_{t_0}^{s} L^1 a(X_z)\,dW_z \right) ds \\ &+ \int_{t_0}^{t} \left(b(X_{t_0}) + \int_{t_0}^{s} L^0 b(X_z)\,dz + \int_{t_0}^{s} L^1 b(X_z)\,dW_z \right) dW_s. \end{aligned}$$

This can simplify to the first-order approximation

$$X_t = X_{t_0} + a(X_{t_0})(t - t_0) + b(X_{t_0})(W_t - W_{t_0}) + R, \tag{6}$$

with the remainder term R consisting of higher-order iterated integrals,

$$\begin{aligned} R \;=\; &\int_{t_0}^{t} \int_{t_0}^{s} L^0 a(X_z)\,dz\,ds + \int_{t_0}^{t} \int_{t_0}^{s} L^1 a(X_z)\,dW_z\,ds \\ &+ \int_{t_0}^{t} \int_{t_0}^{s} L^0 b(X_z)\,dz\,dW_s + \int_{t_0}^{t} \int_{t_0}^{s} L^1 b(X_z)\,dW_z\,dW_s. \end{aligned}$$

Incorporating the next level of expansion further yields

$$X_t = X_{t_0} + a(X_{t_0})(t-t_0) + b(X_{t_0})(W_t - W_{t_0}) + L^1 b(X_{t_0}) \int_{t_0}^{t} \int_{t_0}^{s} dW_z\, dW_s + \bar{R}, \tag{7}$$

with an extended remainder $\bar{R}$,

$$\begin{aligned} \bar{R} \;=\; & \int_{t_0}^{t} \int_{t_0}^{s} L^0 a(X_z)\, dz\, ds + \int_{t_0}^{t} \int_{t_0}^{s} L^1 a(X_z)\, dW_z\, ds \\ & + \int_{t_0}^{t} \int_{t_0}^{s} L^0 b(X_z)\, dz\, dW_s + \int_{t_0}^{t} \int_{t_0}^{s} \int_{t_0}^{z} L^0 L^1 b(X_u)\, du\, dW_z\, dW_s \\ & + \int_{t_0}^{t} \int_{t_0}^{s} \int_{t_0}^{z} L^1 L^1 b(X_u)\, dW_u\, dW_z\, dW_s. \end{aligned}$$

Dropping the remainder term in (6) gives us the Euler–Maruyama method, which is the simplest numerical scheme

$$X_{n+1} = X_n + a(X_n)\Delta t + b(X_n)\Delta W_n, \tag{8}$$

where $\Delta t = t_{n+1} - t_n$ and $\Delta W_n = W_{t_{n+1}} - W_{t_n}$. This scheme has strong order 0.5 and weak order of convergence 1.0. Similarly, the Milstein method is obtained by incorporating the first stochastic correction term and dropping the additional error term in (7)

$$X_{n+1} = X_n + a(X_n)\Delta t + b(X_n)\Delta W_n + \frac{1}{2} b(X_n) b'(X_n) \left((\Delta W_n)^2 - \Delta t \right), \tag{9}$$

which achieves strong and weak order of convrgence of 1.0.

Despite their accuracy, Taylor-based schemes like Milstein require the evaluation of derivatives $b'(x)$, and potentially higher derivatives. This is often impractical because:

- Evaluating multiple derivatives at each step is computationally expensive.
- Derivatives may not be explicitly known or easy to compute.
- Approximating derivatives numerically may introduce errors and complexity.

To overcome these issues, derivative-free methods such as Runge-Kutta schemes for SDEs have been developed. These methods replace derivative evaluations with additional function evaluations of a and b, trading derivative computations for increased function calls. A representative derivative-free Runge-Kutta scheme with explicit strong order 1.0 convergence approximates the derivative $b'(x_i)$ by a finite difference, resulting in:

$$x_{i+1} = x_i + a(x_i)\Delta t_i + b(x_i)\Delta W_i + \frac{1}{2\sqrt{\Delta t_i}} \left[b\left(x_i + b(x_i)\sqrt{\Delta t_i} \right) - b(x_i) \right] \left((\Delta W_i)^2 - \Delta t_i \right).$$

Alternatively, this can be expressed as an implicit version of the Runge-Kutta scheme of strong order 1.0:

$$x_{i+1} = x_i + a(x_i)\Delta t_i + b(x_i)\Delta W_i + \frac{1}{2\sqrt{\Delta t_i}}\left[b(\bar{x}_i) - b(x_i)\right]\left((\Delta W_i)^2 - \Delta t_i\right),$$

where

$$\bar{x}_i = x_i + a(x_i)\Delta t_i + b(x_i)\sqrt{\Delta t_i}.$$

The derivative-free Runge-Kutta schemes maintain the strong convergence order of Milstein without requiring explicit derivative calculations, making them suitable for practical applications where the drift and diffusion functions are complicated or data-driven.

5. Error Metrics, Goodness-of-Fit Test and Convergence Measure

In this study, we applied standard error metrics to evaluate the accuracy of SDE solutions relative to a deterministic benchmark. The Mean Absolute Deviation (MAD) quantifies the average magnitude of errors, regardless of direction. The Mean Absolute Percentage Error (MAPE) provides a normalized measure, expressing errors as percentages, which allows for easier comparison across states with different scales. The Root Mean Square Error (RMSE) emphasizes larger deviations due to squaring the errors, offering insight into overall model precision. In addition to these metrics, we conducted the Anderson-Darling goodness-of-fit (ADG) test as a formal statistical method to assess whether the distribution of the simulated values aligns with that of the deterministic outputs. The ADG test is particularly sensitive to differences in the tails of distributions, making it suitable for detecting subtle deviations in stochastic modeling.

The following deviations, goodness-of-fit and convergence metrics were used to evaluate model performance:

i. Mean Absolute Deviation (MAD).

$$\text{MAD} = \frac{1}{n}\sum_{i=1}^{n}|y_i - \hat{y}_i| \tag{10}$$

MAD measures the average absolute deviation between the observed values y_i and the predicted or reference values $\hat{y}_i$.

ii. Mean Absolute Percentage Error (MAPE).

$$\text{MAPE} = \frac{100\%}{n}\sum_{i=1}^{n}\left|\frac{y_i - \hat{y}_i}{y_i}\right| \tag{11}$$

MAPE provides a normalized measure of prediction error, expressed as a percentage of the true values.

iii. Root Mean Square Error (RMSE).

$$\text{RMSE} = \sqrt{\frac{1}{n}\sum_{i=1}^{n}(y_i - \hat{y}_i)^2} \tag{12}$$

RMSE gives greater weight to larger errors due to squaring the residuals.

iv. Anderson-Darling Goodness-of-Fit (ADG) Test.

$$A^2 = -n - \frac{1}{n}\sum_{i=1}^{n}(2i-1)\left[\ln F(Y_{(i)}) + \ln\left(1 - F(Y_{(n+1-i)})\right)\right] \tag{13}$$

where $Y_{(i)}$ are the ordered observed values, and F is the cumulative distribution function of the theoretical distribution. The ADG test [11] is sensitive to deviations in the tails of the distribution.

v. Okwomi C^* Convergence Measure. Based on Geweke diagnostic [12] that evaluate whether a single chain has reached its convergency by comparing the means of two non-overlapping segments of the chain, we derive a new measure of convergence: Okwomi C^* (C_s^*).

Define:

$$Z = \frac{\bar{X}_a - \bar{X}_b}{\sqrt{\text{Var}(\bar{X}_a) + \text{Var}(\bar{X}_b)}} \tag{14}$$

where:

- $\bar{X}_a$: mean of the early segment (e.g., first 10%),
- $\bar{X}_b$: mean of the late segment (e.g., last 50%),
- $Z \sim \mathcal{N}(0,1)$ under the null hypothesis of convergence.

We define the convergence score as:

$$C = \exp\left(-\frac{Z^2}{2}\right) \tag{15}$$

To scale it to the interval $[0.5, 1.0]$, define new convergence metric named Okwomi C^*:

$$C_s^* = 0.5 + 0.5 \cdot C \tag{16}$$

Interpretation: $C_s^* = 1.0$ shows excellent convergence (agreement in means or variances), and $C_s^* = 0.5$ shows poor convergence (large discrepancy between early and late segments).

6. RESULTS

For the simulations of the malaria dynamics from the SDE model (**??**) we used the parameters shown on Table 1.

TABLE 1. Typical parameter values of SDE SIR malaria model, [13].

Parameter	**Description**	**Parameter Value**
α_h	Natural death rates for humans	0.05
ρ_h	Disease induced death rates for humans	0.0001
δ_h	Infected migration rates for humans	0.1
β_h	Human contact rates	0.01
β_m	Mosquito contact rate	0.05
π_m	Recruitment rate of mosquitoes.	125
α_m	Natural death rates for mosquitoes.	0.06
γ_h	Recovery rates for humans.	0.09
π_h	Recruitment rate of humans.	2.5

Each simulation was initialized with a fixed seed to enable consistent comparison across numerical schemes and ensure result reproducibility. The initial population values at time zero were same across all simulation approaches.

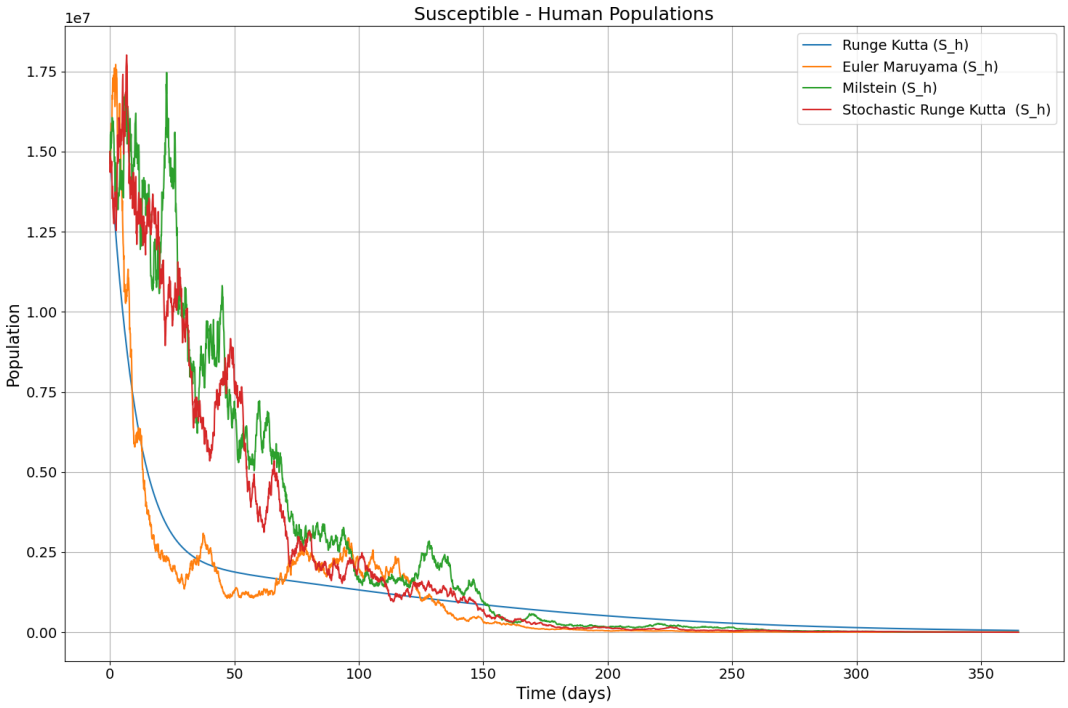

FIGURE 2. Simulated profiles of the susceptible human population using both deterministic and stochastic model fits.

Figure 2 illustrates the dynamics of the susceptible human populations as they evolve over time. Initially, the number of susceptible individuals is high, but as the infection spreads, some individuals transition to the infected category. The Euler–Maruyama method closely follows the trajectory of the deterministic Runge–Kutta solution, indicating strong agreement in their dynamics. In contrast, the Milstein method and the Stochastic Runge–Kutta approach exhibit comparable behaviour to each other, capturing the stochastic variations more similarly while still reflecting the general trend observed in the deterministic solution.

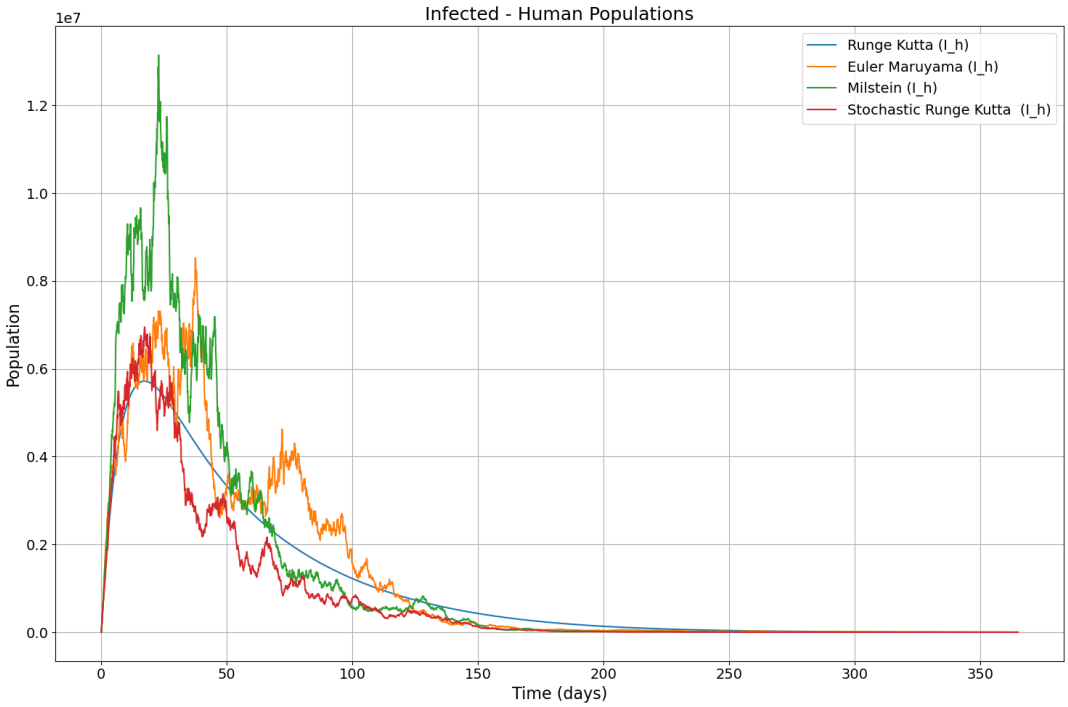

FIGURE 3. Simulated profiles of the infected human population using both deterministic and stochastic model fits.

As can be seen in Figure 3, all the numerical schemes generally align on the trajectory of infected individuals. Although the Milstein method slightly overestimates infections during the early phase, it converges with the other methods after approximately 50 days, maintaining consistency in the overall trend and range of the infection curve across simulation approaches.

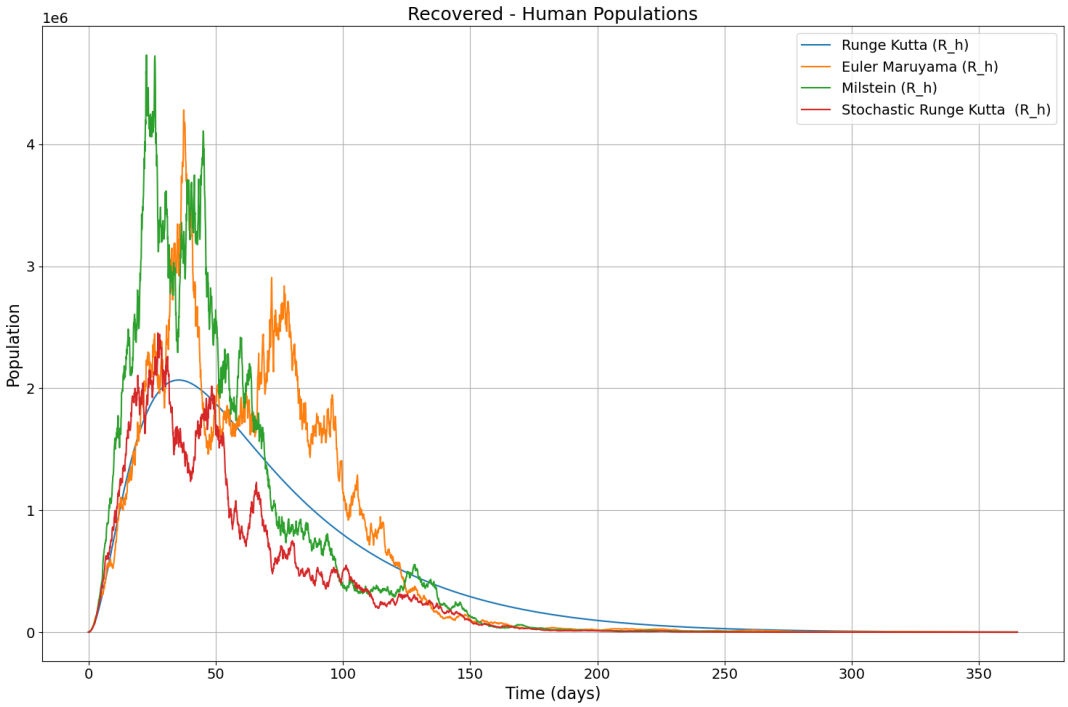

FIGURE 4. Simulated profiles of the recovered human population using both deterministic and stochastic model fits.

Over time, as infected individuals recover and acquire immunity, their numbers increase while the susceptible population decreases. Figure 4 presents the recovered population. The Stochastic Runge–Kutta method tends to underestimate recoveries, while the Milstein method initially overestimates and later underestimates them. Among the methods compared, Euler–Maruyama offers the most consistent and reliable recovery estimates over time, suggesting it may be the most suitable modelling approach.

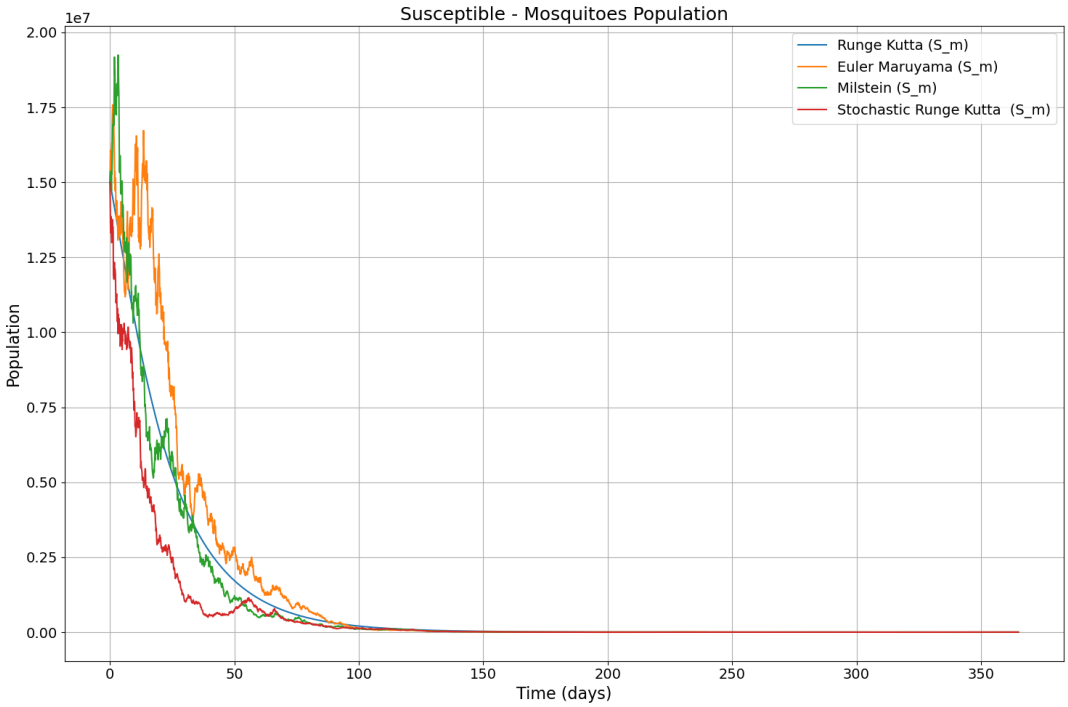

FIGURE 5. Simulated profiles of the susceptible mosquito population using both deterministic and stochastic model fits.

Figure 5 presents the evolution of the susceptible mosquito populations over time. As the transmission cycle advances, the deterministic trajectory lies between the Stochastic Runge–Kutta, which underestimates, and Euler–Maruyama, which tends to overestimate. The Milstein method provides a relatively accurate and balanced estimate of the susceptible mosquito population throughout the simulation period, showing closer alignment with expected dynamics.

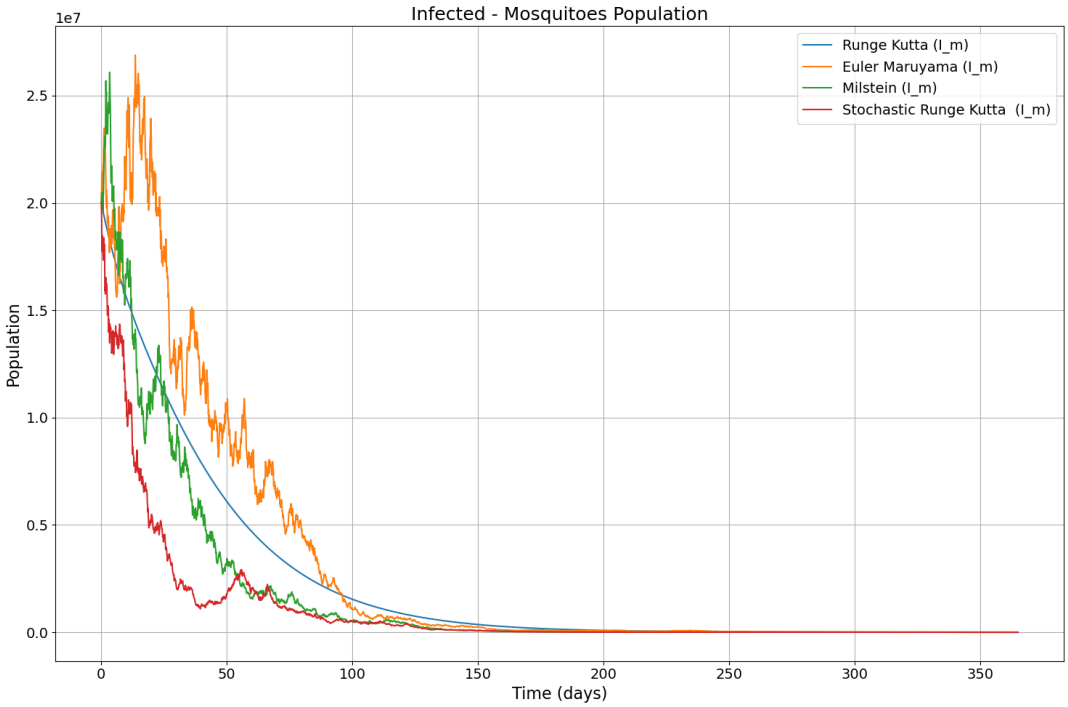

FIGURE 6. Simulated profiles of the infected mosquito population using both deterministic and stochastic model fits.

We evaluated the SDE simulation curves by comparing them against the corresponding deterministic model curve, which served as the gold standard reference. To quantify the accuracy and performance of the SDE approximations, we employed several standard error metrics: MAD, MAPE, and RMSE. These indicators provided a comprehensive assessment of both absolute and relative deviations between the simulated and deterministic outputs. Beyond these conventional performance measures, we also conducted a formal statistical test for distributional similarity—the ADG test. This additional step allowed us to rigorously examine whether the distributions of the SDE solutions statistically align with those from the deterministic framework, offering deeper model validation.

TABLE 2. Error measures and ADF stationary tests for each state using all methods.

State	Method	MAD	MAPE	RMSE	ADF Statistics	ADF p-value	Okwomi C_s^*
S_H	EM	**1283.4**	**67.6**	**35930.1**	-9.09	¡0.001	0.5000
	MI	4089.5	98.9	154765.1	-3.07	0.029	**0.695**
	SRK	3348.1	88.7	129244.9	-4.28	0.001	0.600
I_H	EM	851.6	**39.1**	32866.4	-1.34	**0.609**	**0.778**
	MI	1338.1	65.7	59181.9	-1.58	**0.493**	**0.725**
	SRK	**821.9**	69.1	**25290.3**	-1.95	**0.309**	**0.819**
R_H	EM	**517.1**	**45.1**	**19592.8**	-1.56	**0.505**	**0.732**
	MI	645.3	67.2	25293.5	-1.49	**0.536**	**0.674**
	SRK	472.5	69.1	14032.5	-1.38	**0.674**	**0.758**
S_M	EM	1001.9	35.2	58339.3	-5.7	¡0.001	0.534
	MI	**439.9**	**29.8**	**25200.9**	-14.15	¡0.001	0.505
	SRK	1066.3	39.2	52221.7	-8.52	¡0.001	0.526
I_M	EM	2712.1	**52.4**	119059.4	-3.37	0.012	**0.664**
	MI	**1738.2**	70.9	**61942.6**	-10.76	¡0.001	0.517
	SRK	3245.6	81.7	125421.5	-7.7	¡0.001	0.504

Based on the performance metrics-MAD, MAPE, RMSE-the EM method consistently outperformed the other SDE solvers. It exhibited the lowest error values in most cases, indicating superior accuracy compared to Milstein (MI) and Stochastic Runge-Kutta (SRK) methods, as smaller values in these metrics reflect better performance. Regarding stationarity, the results of all methods confirmed that the time series for infected humans and reverenced humans were stochastic, while the remaining state variables did not display stochastic behaviour. According to the Okwomi C^* convergence measure , most states exhibit convergence, with $C_s^* > 0.50$. Convergence was observed primarily in the states estimated using the Euler–Maruyama and Milstein methods.

7. Conclusion

This study compared the performance of three stochastic numerical schemes-Euler-Maruyama, Milstein, and Stochastic Runge-Kutta-against a deterministic Runge-Kutta baseline in modelling infectious disease dynamics. Initially, susceptible individuals dominate the population, but as infections spread, transitions to the infected class occur. The Euler–Maruyama method showed the closest alignment with the deterministic trajectory, particularly for human infections and recoveries, indicating high consistency and reliability. While the Milstein method exhibited slight overestimation in early phases and underestimation later, it generally produced balanced estimates, especially for susceptible mosquito populations. The Stochastic Runge–Kutta method consistently underestimated key compartments, including infected and recovered individuals. Across simulations, the deterministic trajectory was often bounded between the Euler–Maruyama and Stochastic Runge–Kutta curves. Overall, Euler–Maruyama and Milstein provided the most robust approximations of the deterministic model, with Euler–Maruyama emerging as the most feasible method for capturing recovery dynamics, and Milstein offering a practical balance for both human and vector compartments under stochastic influences. More importantly, as a result of the simulation, we introduced a new convergence metric named Okwomi C^*.

Conflict of Interests

The authors declare that there is no conflict of interests.

References

[1] D. Bernoulli, D. Chapelle, Essai D'une Nouvelle Analyse de la Mortalité Causée par la Petite Vérole, et des Avantages de L'inoculation pour la Prévenir, hal-04100467 (2023). https://inria.hal.science/hal-04100467.

[2] R.M. Anderson, R.M. May, Population Biology of Infectious Diseases: Part I, Nature 280 (1979), 361–367. https://doi.org/10.1038/280361a0.

[3] R.M. May, R.M. Anderson, Population Biology of Infectious Diseases: Part II, Nature 280 (1979), 455–461. https://doi.org/10.1038/280455a0.

[4] W.O. Kermack, A.G. McKendrick, A Contribution to the Mathematical Theory of Epidemics, Proc. R. Soc. Lond. Ser. A 115 (1927), 700–721. https://doi.org/10.1098/rspa.1927.0118.

[5] L.J. Allen, A Primer on Stochastic Epidemic Models: Formulation, Numerical Simulation, and Analysis, Infect. Dis. Model. 2 (2017), 128–142. https://doi.org/10.1016/j.idm.2017.03.001.

[6] D.N. Rusatsi, Bayesian Analysis of Seir Epidemic Models, Thesis, Lappeenranta University of Technology, (2015).

[7] R. Anderson, Infectious Diseases of Humans: Dynamics and Control, Oxford University Press, 1991.

[8] E. Allen, Modeling with Itô Stochastic Differential Equations, Springer, Dordrecht, 2007. https://doi.org/10.1007/978-1-4020-5953-7.

[9] A. Gray, D. Greenhalgh, L. Hu, X. Mao, J. Pan, A Stochastic Differential Equation Sis Epidemic Model, SIAM J. Appl. Math. 71 (2011), 876–902. https://doi.org/10.1137/10081856x.

[10] B. Øksendal, Stochastic Differential Equations, Springer, Berlin, 2013. https://doi.org/10.1007/978-3-662-03620-4.

[11] W.A. Fuller, Introduction to Statistical Time Series, Wiley, 1995. https://doi.org/10.1002/9780470316917.

[12] J. Geweke, Evaluating the Accuracy of Sampling-Based Approaches to the Calculation of Posterior Moments, Bayesian Stat. 4 (1992), 169–194. https://doi.org/10.1093/oso/9780198522669.003.0010.

[13] M. Tilahun, Backward Bifurcation in Sirs Malaria Model, arXiv:1707.00924 (2017). http://arxiv.org/abs/1707.00924v3.